J. Fluid Mech. (1996), vol. 325, pp. 219–237

Effect of laminar chaos on reaction and dispersion in eccentric annular flow

By MICHELLE D. BRYDEN AND HOWARD BRENNER

Department of Chemical Engineering, Massachusetts Institute of Technology, Cambridge, MA 02139-4307, USA

(Received 14 July 1995 and in revised form 13 March 1996)

Generalized Taylor dispersion theory is used to study the chaotic laminar transport of a reactive solute between eccentric rotating cylinders in the presence of an inhomogeneous chemical reaction. The circumstance considered is that of laminar axial 'Poiseuille' flow in the annular region between the two non-concentric cylinders, accompanied by a secondary, generally chaotic, flow induced via alternate rotation of the cylinders. A Brownian tracer introduced into the flow is assumed to undergo an instantaneous, irreversible reaction on the surface of the outer cylinder. The resulting effective transversely and time-averaged reaction rate, axial solute velocity, and axial convective dispersivity are computed. When chaos is present, the effective reaction rate is increased to a value several times larger than occurs in the absence of chaotic transport. It is found that an optimum alternation frequency exists, and that this frequency decreases with increasing transverse Péclet number (Pe_q). It is also observed that the maximum achievable reaction rate increases with Pe_q. The effect of laminar chaotic mixing on the mean axial solute/solvent velocity ratio is to drive its value towards the perfectly mixed value of 1.0, despite the removal of solute from the slower-moving axial streamlines near the outer (reactive) cylinder wall. Lastly, in the presence of transverse chaotic transport, the convective Taylor contribution to the axial solute dispersivity acquires a value up to several orders of magnitude smaller than that achievable by means of non-chaotic convection.

1. Introduction

Much attention has been paid to the use of chaos as a possible mechanism for the enhancement of laminar mixing processes (Ottino 1990; Ottino *et al.* 1992; Aref & Balachandar 1986; Swanson & Ottino 1990). These studies rely heavily on the Poincaré section as a diagnostic to measure the extent of mixing. As pointed out by Swanson & Ottino (1990), however, these diagrams are subject to misinterpretation; nor do they provide any rate information.

The above-cited studies focus on measuring the extent of mixing possible in a chaotic convective flow field, neglecting any effects arising from molecular diffusion. Relatively few studies of the enhancement of transport rates by laminar chaos exist. Jana & Ottino (1992) studied heat transfer in a chaotic cavity flow. They considered the approach to equilibrium of an initially isothermal fluid which is perturbed by a step change in the wall temperature, and found significant enhancement in the rate of heat transfer in circumstances for which chaotic transport is present. The net heat transfer rate exhibited a strong dependence on the Péclet number (Pe), having a maximum at intermediate values of Pe. Ghosh, Chang & Sen (1992) investigated

heat transfer between rotating eccentric cylinders when the cylinders are held at a different temperatures. Although their work was limited to small eccentricities and small oscillations superposed on an otherwise steady rotary flow, conditions under which chaotic transport would be expected to be small, they nevertheless found a significant increase in heat transfer occurring in circumstances where chaotic transport was present.

Jones & Young (1994) studied shear dispersion in a twisted pipe for circumstances wherein chaotic particle trajectories were present. Previous studies of dispersion in curved tubes, involving regular non-chaotic particle trajectories (Nunge, Lin & Gill 1972; Janssen 1976; Johnson & Kamm 1986), found that the secondary flow induced by tube curvature acted to decrease the convective dispersion by a factor of up to five below that occurring in a straight tube under comparable conditions. Jones & Young (1994) concluded that the presence of chaotic advection decreases the axial dispersion to an even larger extent than does regular secondary flow, changing the dependence of the dispersivity upon the Péclet number from the classical Pe^2 behaviour (Taylor 1953) to $Pe \ln Pe$.

The present work utilizes Taylor dispersion theory for time-periodic chemically reactive systems (Shapiro & Brenner 1990) to assess the effect of laminar chaos on both transverse and axial solute transport rates. The situation considered is that of net axial annular flow taking place between eccentric cylinders which are alternately rotated. This flow has been studied both experimentally and computationally by Kusch & Ottino (1992). In addition, flow between rotating eccentric cylinders (in the absence of axial flow) has been studied extensively as a simple example of a system in which the phenomenon of laminar chaos occurs under well-defined conditions (Aref & Balachandar 1986; Chaiken *et al.* 1987; Swanson & Ottino 1990; Kaper & Wiggins 1993). A Brownian tracer particle, likened to a diffusing solute molecule, is assumed to undergo instantaneous irreversible reaction on the outer cylinder surface† following its initial introduction into the annular space between the cylinders. A global, purely axial, transversely and time-averaged description of the resulting reactive transport process is sought and ultimately found. In particular, the effective reaction or wall deposition rate, mean axial solute velocity, and axial dispersivity are computed. Since the deposition is assumed instantaneous, its rate is limited by the transport of solute to the wall rather than by the true kinetics of the reaction or deposition process. Hence, the effective reaction rate furnishes a quantitative global measure of the transport effectiveness in a given secondary (i.e. transverse) flow field. The convective or Taylor contribution to the axial dispersivity also depends on the lateral transport, varying inversely with molecular diffusivity in a purely axial flow. Thus, the effect of any enhancement in the net transverse transport is to decrease the axial dispersion, whence the latter also furnishes an additional, independent measure of the transport effectiveness of a given chaotic flow field.

2. Geometry and flow

Consider an infinitely long circular cylinder of radius R_i positioned non-concentrically within another, larger cylinder of radius R_o, their centres being separated by a distance ε (figure 1). (Throughout, subscripts i and o represent the values of

† We will on occasion refer to this instantaneous irreversible process as 'deposition', having in mind the model of a Brownian aerosol or hydrosol particle being deposited on the outer wall and held there permanently (Shapiro & Brenner 1986; Shapiro, Kettner & Brenner 1991).

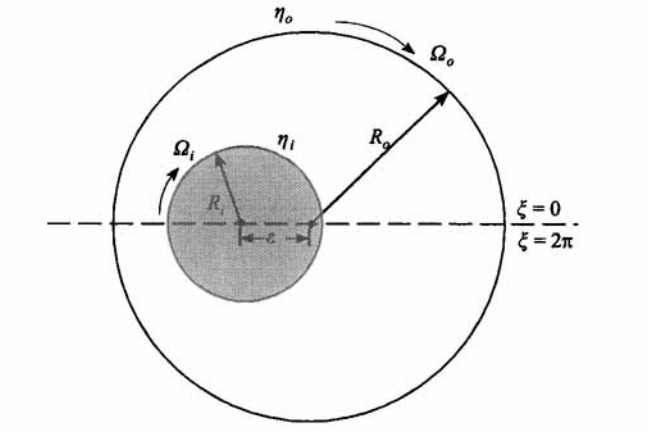

FIGURE 1. Eccentric cylinders. Bipolar coordinates.

the functions to which they are affixed on the inner and outer cylinders, respectively.) A point within the eccentric annular space bounded by the two cylinders will be denoted $(z, \boldsymbol{q})$, with z the axial position parallel to the cylinder axes, and $\boldsymbol{q} \equiv \boldsymbol{q}(\eta, \xi)$ the 'local', transverse position vector in the plane perpendicular to the z-axis. Here, η and ξ are cylindrical curvilinear coordinates, explicitly bipolar coordinates in the present context (Happel & Brenner 1983).

A transverse flow is produced by rotating the inner and outer cylinders alternately, each for the same period T at the respective angular velocities Ω_i and Ω_o. The secondary, local-space velocity field is then given by

$$\boldsymbol{u}(\boldsymbol{q}, t) = \begin{cases} \boldsymbol{u}_i(\boldsymbol{q}), & 2nT < t < (2n+1)T, \\ \boldsymbol{u}_o(\boldsymbol{q}), & (2n+1)T < t < 2(n+1)T \end{cases} \tag{2.1}$$

$(n = 0, 1, 2, ...)$, where $\boldsymbol{u}_i$ and $\boldsymbol{u}_o$ are the quasi-steady Stokes-flow bipolar-coordinate velocity fields (Ballal & Rivlin 1976) respectively resulting from rotation of the inner and outer cylinders. The quasi-steady assumption is valid provided that the period of modulation T is large compared with the viscous time scale L^2/ν, where L is a characteristic length, say $R_o - R_i$, and ν the kinematic viscosity. The assumption of Stokes flow is justified provided the Reynolds number $Re = R^2\Omega/\nu$ is less than unity (San Andres & Szeri 1984).

In addition to the unsteady two-dimensional transverse flow produced by the rotation of the cylinders, a steady laminar axial flow $\boldsymbol{U} = \boldsymbol{i}_z U(\boldsymbol{q})$ is superposed. This Poiseuille-like bipolar-coordinate flow field is given by Snyder & Goldstein (1965), among others (Piercy, Hooper & Winney 1933).

3. Probability density transport

Consider an effectively point-size Brownian solute particle introduced at time t' into the flow $\boldsymbol{U} + \boldsymbol{u}$ occurring between the two eccentric cylinders. The particle will be assumed to undergo transport by convection and diffusion in the annular space while undergoing instantaneous, irreversible deposition on the outer cylinder. Let $P \equiv P(z, \boldsymbol{q}, t|\boldsymbol{q}', t')$ denote the conditional probability density that the tracer is located at the point $(z, \boldsymbol{q})$ at time t, given that it was initially introduced into the fluid at the point $(0, \boldsymbol{q}')$ at time t'. This probability density is governed by the following

boundary-value problem:

$$\frac{\partial P}{\partial t} + U(\boldsymbol{q})\frac{\partial P}{\partial z} + \boldsymbol{u}(\boldsymbol{q},t)\cdot\nabla_q P - D\left(\frac{\partial^2 P}{\partial z^2} + \nabla_q^2 P\right) = \delta(z)\delta(\boldsymbol{q}-\boldsymbol{q}')\delta(t-t'), \tag{3.1}$$

$$P = 0 \quad \text{on} \quad \partial\boldsymbol{q}_o, \tag{3.2}$$

$$\boldsymbol{n}\cdot\nabla_q P = 0 \quad \text{on} \quad \partial\boldsymbol{q}_i, \tag{3.3}$$

$$|z|^m P \to 0 \quad \text{as} \quad z \to \pm\infty \quad (m = 0, 1, 2, \ldots). \tag{3.4}$$

Here, D is the molecular diffusivity, ∇_q the local-space (two-dimensional) gradient operator, $\boldsymbol{n}$ the unit normal vector, and $\partial\boldsymbol{q}_\alpha$ a point lying on the surface of a circular cylinder, η_α = constant ($\alpha = i, o$). Boundary condition (3.2) is a consequence of the instantaneous irreversible solute deposition on the outer cylinder, while (3.3) represents the condition of no flux through the inner cylinder wall. Equation (3.4) is necessitated by the requirement that the probability density be bounded as $|z| \to \infty$ in such a way that the axial moment integrals

$$\int_{-\infty}^{\infty} z^m P \,\mathrm{d}z \tag{3.5}$$

implicit in the subsequent theory converge for all non-negative integers m and for all local points $\boldsymbol{q} \in \boldsymbol{q}_0$, in which $\boldsymbol{q}_0$ represents the two-dimensional annular domain ($0 \leqslant \xi < 2\pi$, $\eta_o \leqslant \eta \leqslant \eta_i$) lying perpendicular to the axes of the cylinders, η_i and η_o.

4. Global, axial transport description

A macroscale description of the transport processes outlined above may be obtained through application of the time-periodic moment-matching scheme described by Shapiro & Brenner (1990). This method allows the calculation of mean transport coefficients which are independent of the exact initial conditions, thus providing global information about the transport processes and eliminating the necessity of performing a separate calculation for each new set of initial conditions.

Define the time- and transverse-position-averaged conditional probability density

$$\langle\bar{P}\rangle(z,t|\boldsymbol{q}',t') = \frac{1}{2T}\int_t^{t+2T}\int_{\boldsymbol{q}_0} P(z,\boldsymbol{q},t|\boldsymbol{q}',t')\mathrm{d}\boldsymbol{q}\,\mathrm{d}t. \tag{4.1}$$

Here, the transverse average of a function $f(z,\boldsymbol{q},t)$ is defined as

$$\bar{f}(z,t) = \int_{\boldsymbol{q}_0} f(z,\boldsymbol{q},t)\mathrm{d}\boldsymbol{q}, \tag{4.2}$$

whereas

$$\langle f\rangle(z,\boldsymbol{q},t) = \frac{1}{2T}\int_t^{t+2T} f(z,\boldsymbol{q},t)\mathrm{d}t \tag{4.3}$$

denotes the time-average of the function over one period, $2T$. For asymptotically long times $\langle\bar{P}\rangle$ obeys the following one-dimensional system of macroscale, axial convection–dispersion–(first-order, irreversible) reaction equations (Shapiro & Brenner 1990):

$$\frac{\partial\langle\bar{P}\rangle}{\partial t} + \bar{U}^*\frac{\partial\langle\bar{P}\rangle}{\partial z} - \bar{D}^*\frac{\partial^2\langle\bar{P}\rangle}{\partial z^2} + \bar{K}^*\langle\bar{P}\rangle = A(\boldsymbol{q}',t')\delta(z)\delta(t-t'), \tag{4.4}$$

$$|z|^m\langle\bar{P}\rangle \to 0 \quad \text{as} \quad z \to \pm\infty. \tag{4.5}$$

The macroscale phenomenological coefficients $\bar{K}^*, \bar{U}^*$, and $\bar{D}^*$ respectively represent the effective solute reaction-rate constant, axial velocity, and axial dispersivity. These axial position- and time-independent constants are given in terms of quadratures of the microscale phenomenological and geometric data by the expressions

$$\bar{K}^* = K, \tag{4.6}$$

$$\bar{U}^* = \frac{1}{2T}\int_0^{2T}\int_{\boldsymbol{q}_0} U(\boldsymbol{q})P_0^\infty(\boldsymbol{q},t)A(\boldsymbol{q},t)\mathrm{d}\boldsymbol{q}\,\mathrm{d}t \tag{4.7}$$

and

$$\bar{D}^* = D + \bar{D}_c^*, \tag{4.8}$$

where

$$\bar{D}_c^* = \frac{1}{2T}\int_0^{2T}\int_{\boldsymbol{q}_0} B(\boldsymbol{q},t)P_0^\infty(\boldsymbol{q},t)A(\boldsymbol{q},t)[U(\boldsymbol{q}) - \bar{U}^*]\mathrm{d}\boldsymbol{q}\,\mathrm{d}t \tag{4.9}$$

is the Taylor (i.e. 'convective') contribution to the axial dispersivity. Here, the local-space P_0^∞ and A fields together with the reactivity coefficient K are found from the following adjoint pair of transverse-space eigenvalue problems:

$$\frac{\partial P_0^\infty}{\partial t} + \boldsymbol{u}\cdot\nabla_q P_0^\infty - D\nabla_q^2 P_0^\infty - K P_0^\infty = 0, \tag{4.10}$$

$$P_0^\infty = 0 \quad \text{on} \quad \partial\boldsymbol{q}_o, \tag{4.11}$$

$$\boldsymbol{n}\cdot\nabla_q P_0^\infty = 0 \quad \text{on} \quad \partial\boldsymbol{q}_i, \tag{4.12}$$

$$P_0^\infty(\boldsymbol{q}, t+2T) = P_0^\infty(\boldsymbol{q}, t), \tag{4.13}$$

$$\frac{1}{2T}\int_t^{t+2T}\int_{\boldsymbol{q}_0} P_0^\infty \mathrm{d}\boldsymbol{q}\,\mathrm{d}t = 1; \tag{4.14}$$

and

$$\frac{\partial A}{\partial t} + \boldsymbol{u}\cdot\nabla_q A + D\nabla_q^2 A + KA = 0, \tag{4.15}$$

$$A = 0 \quad \text{on} \quad \partial\boldsymbol{q}_o, \tag{4.16}$$

$$\boldsymbol{n}\cdot\nabla_q A = 0 \quad \text{on} \quad \partial\boldsymbol{q}_i, \tag{4.17}$$

$$A(\boldsymbol{q}, t+2T) = A(\boldsymbol{q}, t), \tag{4.18}$$

$$\int_{\boldsymbol{q}_0} P_0^\infty A \mathrm{d}\boldsymbol{q} = 1. \tag{4.19}$$

The B field required in the determination of $\bar{D}^*$ represents the solution of the following boundary-value problem:

$$\frac{\partial(BP_0^\infty)}{\partial t} + \boldsymbol{u}\cdot\nabla_q(BP_0^\infty) - D\nabla_q^2(BP_0^\infty) - KBP_0^\infty = P_0^\infty[U(\boldsymbol{q}) - \bar{U}^*], \tag{4.20}$$

$$BP_0^\infty = 0 \quad \text{on} \quad \partial\boldsymbol{q}_o, \tag{4.21}$$

$$\boldsymbol{n}\cdot\nabla_q(BP_0^\infty) = 0 \quad \text{on} \quad \partial\boldsymbol{q}_i. \tag{4.22}$$

The term appearing on the right-hand side of (4.4) represents a 'fictitious' initial condition, which differs from the true, delta-function initial condition by the factor $A(\boldsymbol{q}', t')$. The need for such a fictitious initial condition arises from the fact (Shapiro & Brenner 1990) that the macroscale equation (4.4) is valid only for asymptotically

long times, and hence does not accurately describe the transport occurring at short times. Use of a fictitious initial condition corrects for this 'anomalous' behaviour by properly accounting for the solute transport and reaction occurring *prior* to the time at which the macroscale equation (4.4) becomes applicable. As a result of this initial condition, $\langle \bar{P} \rangle$ depends upon both the initial transverse position $\boldsymbol{q}'$ and the initial time t' (the latter through the combination $t - t'$), although the macroscale phenomenological coefficients $\bar{K}^*$, $\bar{U}^*$, and $\bar{D}^*$ appearing in (4.4) are independent of the initial conditions. The value of $A(\boldsymbol{q}', t')$ may be used to determine the utility of the present asymptotic analysis. In instances in which most of the solute has already been consumed by chemical reaction prior to this asymptotic analysis becoming valid, $A(\boldsymbol{q}', t')$ will be extremely small and the distinction between a small amount of solute remaining and zero residual solute will be negligible from a practical point of view. In other instances, such as when the solute is initially introduced in a region relatively distant from the reactive wall, $A(\boldsymbol{q}', t')$ will be close to unity. Thus, our macroscale analysis will possess greater utility in practical applications. However, practical considerations aside, our analysis nevertheless provides a simple quantitative measure of the effectiveness of laminar chaos in enhancing the transverse transport rate.

Introduce the dimensionless variables

$$\left.\begin{aligned} &\tau = \frac{tD}{R_o^2}, \quad Pe_q = \frac{\bar{u}R_o}{D}, \quad Pe_Q = \frac{\bar{V}R_o}{D}, \quad \kappa = \frac{KR_o^2}{D}, \quad \hat{\boldsymbol{u}} = \frac{\boldsymbol{u}}{\bar{u}}, \\ &\hat{U} = \frac{U}{\bar{V}}, \quad \hat{B} = \frac{B}{R_o Pe_Q}, \quad \hat{P}_0^\infty = P_0^\infty R_o^2, \quad \hat{\nabla}_q = R_o \nabla_q, \end{aligned}\right\} \tag{4.23}$$

in which

$$\bar{u} = \Omega_o R_o \tag{4.24}$$

is the circumferential velocity of the outer cylinder, and

$$\bar{V} = \int_{\boldsymbol{q}_0} U(\boldsymbol{q}) \mathrm{d}\boldsymbol{q} \Big/ \int_{\boldsymbol{q}_0} \mathrm{d}\boldsymbol{q} \tag{4.25}$$

is the average axial solvent velocity. (The denominator of (4.25) is simply the cross-sectional area $\pi(R_o^2 - R_i^2)$ of the annular domain.) This yields the following non-dimensional system of differential equations governing the fields $\hat{P}_0^\infty$, A, and $\hat{B}$:

$$\frac{\partial \hat{P}_0^\infty}{\partial \tau} + Pe_q \hat{\boldsymbol{u}} \cdot \hat{\nabla}_q \hat{P}_0^\infty - \hat{\nabla}_q^2 \hat{P}_0^\infty - \kappa \hat{P}_0^\infty = 0, \tag{4.26}$$

$$\frac{\partial A}{\partial \tau} + Pe_q \hat{\boldsymbol{u}} \cdot \hat{\nabla}_q A + \hat{\nabla}_q^2 A + \kappa A = 0, \tag{4.27}$$

$$\frac{\partial (\hat{B}\hat{P}_0^\infty)}{\partial \tau} + Pe_q \hat{\boldsymbol{u}} \cdot \hat{\nabla}_q (\hat{B}\hat{P}_0^\infty) - \hat{\nabla}_q^2 (\hat{B}\hat{P}_0^\infty) - \kappa \hat{B}\hat{P}_0^\infty = \hat{P}_0^\infty \left(\hat{U}(\boldsymbol{q}) - \frac{\bar{U}^*}{\bar{V}} \right), \tag{4.28}$$

which are to be solved subject to the boundary conditions given by (4.11)–(4.14), (4.16)–(4.19), and (4.21)–(4.22), respectively, with B replaced by $\hat{B}$ and P_0^∞ by $\hat{P}_0^\infty$. In addition, for the macroscale coefficients, one obtains

$$\frac{\bar{U}^* R_0}{D} = \frac{Pe_Q}{2\Upsilon} \int_0^{2\Upsilon} \int_{\boldsymbol{q}_0} \hat{U}(\boldsymbol{q}) \hat{P}_0^\infty(\boldsymbol{q}, \tau) A(\boldsymbol{q}, \tau) \mathrm{d}\boldsymbol{q}\, \mathrm{d}\tau \tag{4.29}$$

and

$$\frac{\bar{D}_c^*}{D} = \frac{Pe_Q^2}{2\Upsilon}\int_0^{2\Upsilon}\int_{q_0}\hat{B}(\boldsymbol{q},\tau)\hat{P}_0^{\infty}(\boldsymbol{q},\tau)A(\boldsymbol{q},\tau)\left(\hat{U}(\boldsymbol{q}) - \frac{\bar{U}^*}{\bar{V}}\right)\mathrm{d}\boldsymbol{q}\,\mathrm{d}\tau, \tag{4.30}$$

in which $\Upsilon = TD/R_0^2$. The relevant parameters to be investigated in quantifying $\bar{K}^*$, $\bar{U}^*$, and $\bar{D}_c^*$ are thus Pe_q, Υ, and Ω_i/Ω_o, in addition to the geometric factors R_i/R_o and (dimensionless) eccentricity $\epsilon = \varepsilon/(R_o - R_i)$.

5. Solution scheme

In order to facilitate determining the eigenvalue κ – representing the effective Damköhler number for the reaction – define the field $p_0^{\infty}(\boldsymbol{q},t)$ as follows:

$$\hat{P}_0^{\infty}(\boldsymbol{q},\tau) = p_0^{\infty}(\boldsymbol{q},\tau)\exp(\kappa\tau). \tag{5.1}$$

From (4.26), the p_0^{∞} field is thus governed by the relation

$$\frac{\partial p_0^{\infty}}{\partial\tau} + Pe_q\hat{\boldsymbol{u}}\cdot\hat{\nabla}_q p_0^{\infty} - \hat{\nabla}_q^2 p_0^{\infty} = 0, \tag{5.2}$$

whereas the equation for the $\hat{B}$ field becomes

$$\frac{\partial(\hat{B}p_0^{\infty})}{\partial\tau} + Pe_q\hat{\boldsymbol{u}}\cdot\hat{\nabla}_q(\hat{B}p_0^{\infty}) - \hat{\nabla}_q^2(\hat{B}p_0^{\infty}) = p_0^{\infty}\left(\hat{U}(\boldsymbol{q}) - \frac{\bar{U}^*}{\bar{V}}\right). \tag{5.3}$$

In terms of the new variables, κ is now given by

$$\kappa = -\lim_{\tau\to\infty}\frac{1}{2\Upsilon}\ln\left(\frac{\int_{q_0} p_0^{\infty}(\boldsymbol{q},\tau+2\Upsilon)\mathrm{d}\boldsymbol{q}}{\int_{q_0} p_0^{\infty}(\boldsymbol{q},\tau)\mathrm{d}\boldsymbol{q}}\right). \tag{5.4}$$

Similarly, upon replacing A by

$$A(\boldsymbol{q},\tau) = a(\boldsymbol{q},\tau)\exp(-\kappa\tau), \tag{5.5}$$

the new field a obeys the equation

$$\frac{\partial a}{\partial\tau} + Pe_q\hat{\boldsymbol{u}}\cdot\hat{\nabla}_q a + \hat{\nabla}_q^2 a = 0. \tag{5.6}$$

The trio of boundary-value problems posed in the preceding paragraph were solved sequentially. Spatially uniform initial conditions were imposed upon each of the above three functions and calculations carried out until each attained its asymptotic, time-periodic behaviour, which was independent of the arbitrarily chosen initial conditions. In order to avoid instabilities associated with (5.6), a new time variable $\theta = -\tau$ was introduced, yielding the following stable equation for $a(\boldsymbol{q},\theta)$:

$$\frac{\partial a}{\partial\theta} - Pe_q\hat{\boldsymbol{u}}\cdot\hat{\nabla}_q a - \hat{\nabla}_q^2 a = 0. \tag{5.7}$$

This equation is identical to that governing the p_0^{∞} field, with the exception of the algebraic sign of the convective term. Owing to the symmetry of the problem, it was not necessary to solve for the a and p_0^{∞} fields separately. Rather, the a field was obtained by inverting the p_0^{∞} field about the axis joining the centres of the two cylinders while reversing its time dependence.

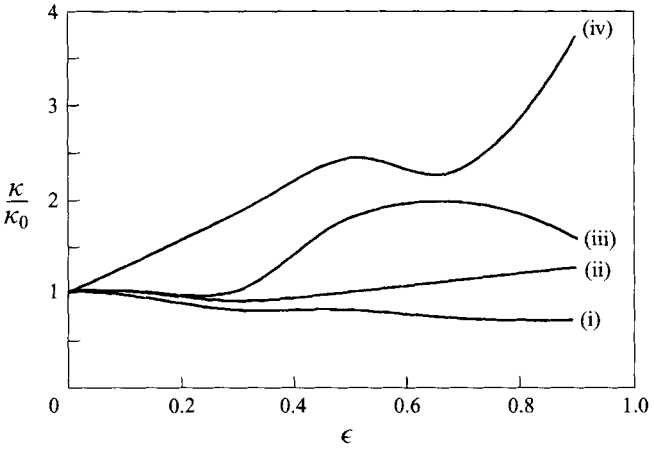

FIGURE 2. Dependence of the ratio of the effective Damköhler number κ to its value κ_0 at zero eccentricity and in the absence of transverse flow on the dimensionless eccentricity ϵ for $R_i/R_o = 0.3$: (i) no transverse flow; (ii–iv): $Pe_q = 5000$, $\Omega_i/\Omega_o = 6$, with (ii) outer cylinder rotation; (iii) inner cylinder rotation; (iv) alternate rotation, $\Upsilon = 0.001$.

The equations were explicitly written in bipolar coordinates (η, ξ) and subsequently solved by an implicit finite-difference method. All the calculations utilized a radius ratio value of $R_i/R_o = 0.3$, while the other parameters were varied over appropriate ranges. First, the eccentricity was varied over its entire range $(0 < \epsilon < 1)$, from the concentric- to the tangent-cylinder case. Pe_q was varied over the range zero to 10^6; large transverse Péclet numbers are of particular interest because species possessing small molecular diffusivities experience extremely small effective reaction rates in the absence of transverse convection, thus making lateral transport enhancement essential in attempting to achieve more rapid reaction rates. In addition to varying Pe_q, which is equivalent to varying the angular velocities of both cylinders, we also studied the effect of the angular velocity ratio Ω_i/Ω_o, including distinguishing between co-rotating cylinders $(\Omega_i/\Omega_o > 0)$ and counter-rotating cylinders $(\Omega_i/\Omega_o < 0)$. Varying this ratio over a range similar to that employed for Pe_q allowed us to assess the effect of varying the velocity of the inner cylinder, while holding the velocity of the outer cylinder fixed. Finally, the alternation period Υ was varied over the range 10^{-5} to 1, respectively corresponding to very rapid oscillation and to a period equal to the diffusion time.

6. Results

6.1. *Reactivity coefficient*

Figure 2 illustrates the dependence of the effective reaction-rate coefficient on the eccentricity, while figure 3 shows representative streamlines for these flow conditions. Figure 2 reveals that in the absence of any flow (curve i), the net deposition rate decreases slightly with increasing eccentricity. This simply reflects the increasing average distance that a particle must travel in order to reach the reactive outer wall. Rotation of the outer cylinder singly (curve ii) leads to only a modest increase in the reaction rate over that in the absence of transverse flow. This increase is due to the separation occurring on the inner cylinder (see figure 3*a*), which serves to transport the reactive species from the area adjacent to the inner cylinder to the central region, thereby increasing the gradient driving the diffusion towards the outer

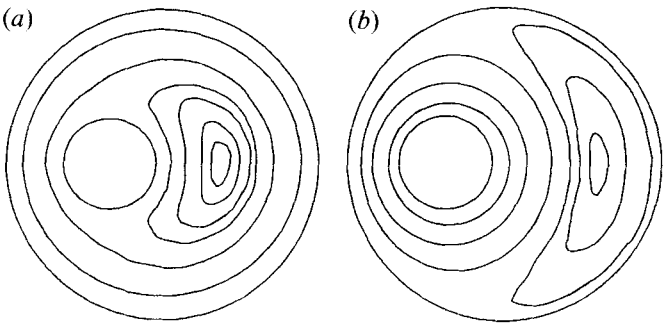

FIGURE 3. Streamlines for $R_i/R_o = 0.3$, $\epsilon = 0.5$: (*a*) outer cylinder rotation, (*b*) inner cylinder rotation.

wall. In comparison with the preceding case of rotation of the outer cylinder, a much more dramatic increase in the deposition rate is observed when the inner cylinder is rotated singly (curve iii). This is a consequence of the location of the separation point. When the inner cylinder is rotated, separation occurs at the outer, reactive wall (see figure 3*b*). Thus, the effect of the separation is to transport species from the central portion of the annulus to the region very close to the reaction site, greatly enhancing the effective reaction rate.

The remaining curve displayed in figure 2 (curve iv) represents a situation in which the cylinders rotate alternately – circumstances for which chaotic advection has been shown to occur (Aref & Balachandar 1986; Chaiken *et al.* 1987; Swanson & Ottino 1990). When each cylinder is successively rotated for a period $\Upsilon = 0.001$, the deposition rate attains a value above that which could be achieved solely from rotation of the inner cylinder alone (curve iii). This clearly demonstrates the transport enhancement occasioned by laminar chaos for this set of parameters. Comparison of the Poincaré sections (figure 4) for these parameters with the resulting deposition rate shows that while there is some relationship between the Poincaré sections and the deposition rate, the conclusions drawn from these diagrams may be different than the calculated results. For instance, a large island is present in the Poincaré section for $\epsilon = 0.7$, suggesting that the mixing achieved in this geometry is less effective than that for either $\epsilon = 0.3$ or $\epsilon = 0.5$, where the only regular regions occur in thin bands close to the outer cylinder. In contrast, the calculated results show that the effective reaction rate for $\epsilon = 0.7$ is only slightly smaller than that for $\epsilon = 0.5$ and is, in fact, larger than that for $\epsilon = 0.3$.

The effect of the alternation period Υ on the deposition rate is illustrated in figure 5. It is seen that an enhanced deposition rate, over that attained by simply rotating the inner cylinder continuously, occurs only over a limited range of frequencies, a result similar to that observed by Ghosh *et al.* (1992) in their study of heat transfer. The increase observed in the deposition rate with switching period for small periods may be explained by examining the Poincaré sections for these flow conditions (figure 6). There is a dramatic increase in the extent of the chaotic regions at the smallest periods (compare figures 6*a* and 6*b*). For longer periods, no such explanation is possible, since here the extent of chaotic regions is comparable to that present at the optimum alternation period. One possible explanation is that for these longer switching periods it takes longer for a comparable amount of mixing to occur, thus decreasing the effective reaction rate. Another possibility is that when molecular diffusion is present, very long switching periods allow sufficient time for

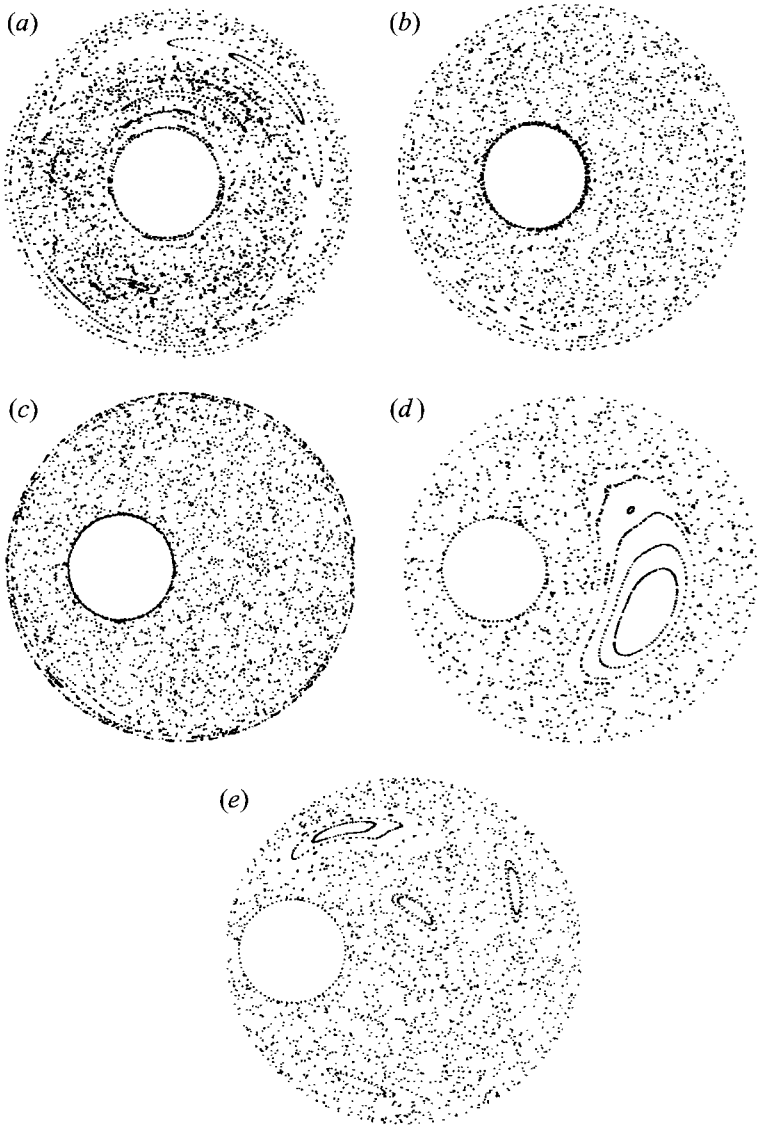

FIGURE 4. Poincaré sections for alternate rotation, with $R_i/R_o = 0.3$, $Pe_q = 5000$, and $\Upsilon = 0.001$: (a) $\epsilon = 0.1$, (b) $\epsilon = 0.3$, (c) $\epsilon = 0.5$, (d) $\epsilon = 0.7$, (e) $\epsilon = 0.9$.

diffusive transport to establish a pseudo-steady state during each half of the cycle, corresponding to that which occurs when one cylinder rotates continuously. The net rate of transport to the outer cylinder is thus (approximately) simply the average of the respective rates attained when each cylinder is rotated individually.

Figure 7 displays the dependence of deposition rate on transverse Péclet number. In the absence of diffusion, Aref & Balachandar (1986) and Chaiken *et al.* (1987) observed that the extent of mixing depends only on the products $\Omega_i T$ and $\Omega_o T$ (i.e., the angular distances travelled by each cylinder during one period) rather than on the angular velocity and switching period individually. Here, the rate depends on each of these parameters separately, as can be seen by comparing figures 5 and 7, which would be the same if the rate depended only on the total distance travelled

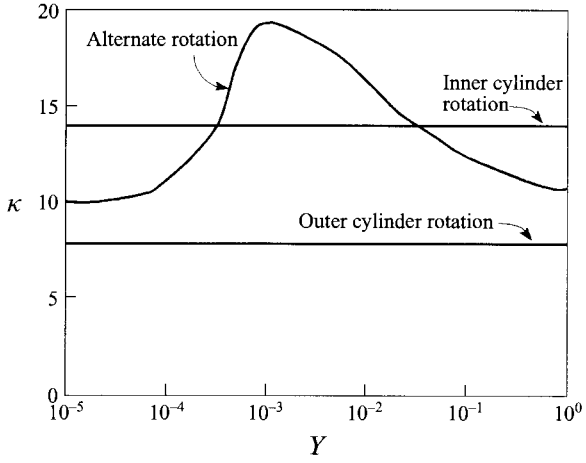

FIGURE 5. Dependence of the effective Damköhler number κ on the alternation period Υ for $R_i/R_o = 0.3$, $\epsilon = 0.5$, $\Omega_i/\Omega_o = 6$, $Pe_q = 5000$.

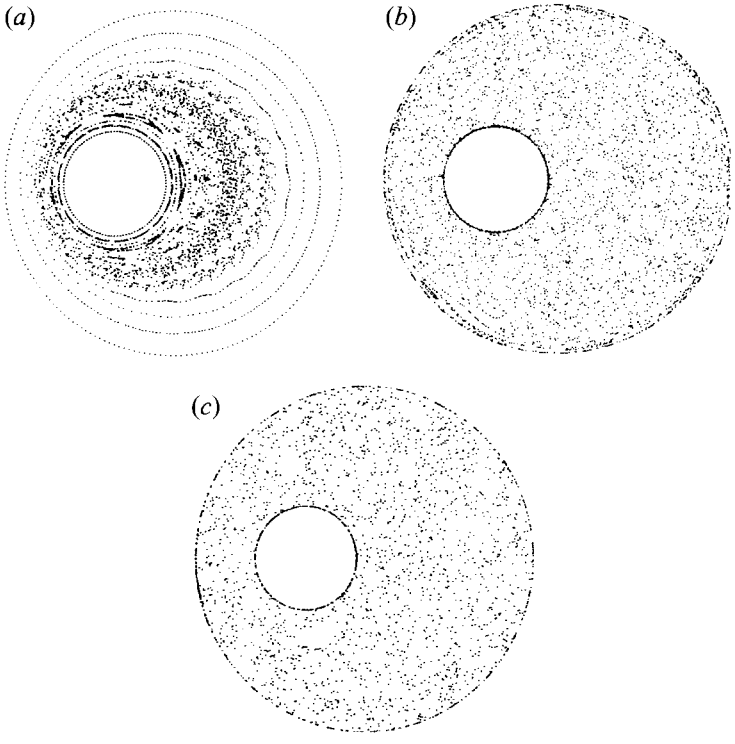

FIGURE 6. Poincaré sections for alternate rotation, with $R_i/R_o = 0.3$, $Pe_q = 5000$, and $\epsilon = 0.5$: (*a*) $\Upsilon = 0.0001$ (*b*) $\Upsilon = 0.001$ (*c*) $\Upsilon = 0.01$

during each period. It is seen that for $Pe_q \lesssim 500$, the deposition rate for alternate rotation falls into the envelope between the respective rates attained for continuous, single-cylinder rotation. For large Péclet numbers the deposition rate reaches an asymptotic value 1.3 times that attained by rotating only the inner cylinder, and 2.5 times that achieved in the complete absence of convection ($Pe_q = 0$).

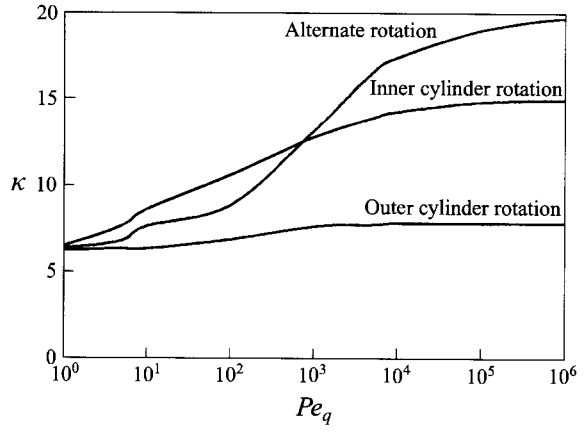

FIGURE 7. Dependence of the effective Damköhler number κ on Pe_q for $R_i/R_o = 0.3$, $\epsilon = 0.5$, $\Omega_i/\Omega_o = 6$, $\Upsilon = 0.01$.

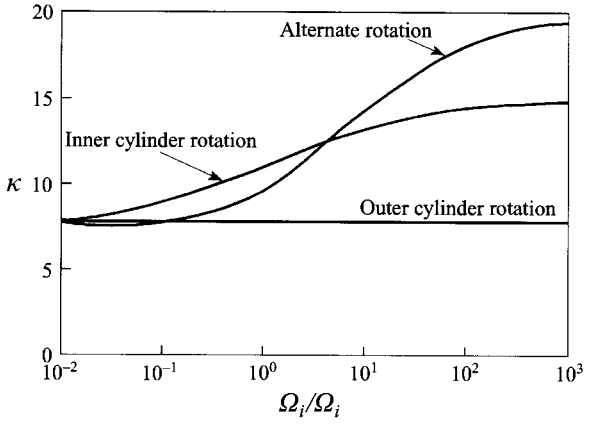

FIGURE 8. Dependence of the effective Damköhler number κ on the angular velocity ratio Ω_i/Ω_o for $R_i/R_o = 0.3$, $\epsilon = 0.5$, $Pe_q = 1000$, $\Upsilon = 0.01$

Figure 8 depicts the effect of varying the angular velocity Ω_i of the inner cylinder, while keeping constant both the switching period Υ and the angular velocity Ω_o of the outer cylinder. Comparison of these results with those observed when the velocities of both cylinders are varied (figure 7) shows that the asymptotic limit for the deposition rate is independent of the angular velocity of the outer cylinder. Moreover, the value of the parameter $Pe_q\Omega_i/\Omega_o$ at which the deposition rate in the presence of chaotic mixing first exceeds that achieved through rotation of the inner cylinder alone is independent of whether the angular velocity of only the inner cylinder or the angular velocities of both cylinders are varied. It thus appears that for large Péclet numbers the rotation rate of the inner cylinder alone controls the deposition rate. This is physically reasonable, since it is the rotation of the inner cylinder that creates a separation region near the outer (reactive) wall. Rotation of the outer cylinder contributes little to the enhancement of the deposition rate on its own, but in combination with alternate rotation of the inner cylinder it serves to transport solute particles from areas lying outside of the separation region to the area of separation, where the local deposition rate is higher. Also investigated was the effect of rotating

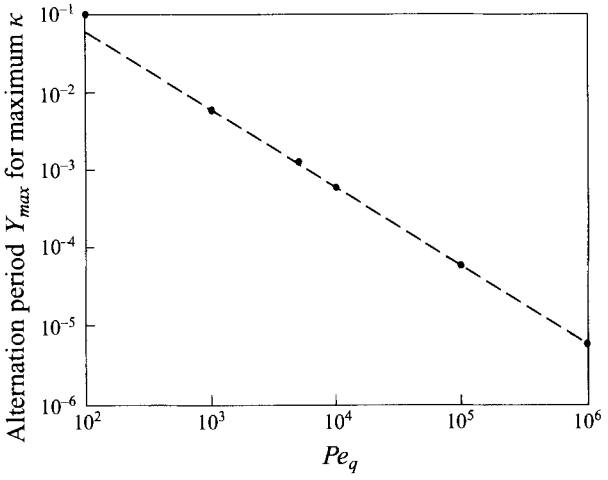

FIGURE 9. Dependence upon Pe_q of the alternation period at which the maximum effective Damköhler number is achieved, with $R_i/R_o = 0.3$, $\epsilon = 0.5$, $\Omega_i/\Omega_o = 6$. The slope of the line is -1.0

the cylinders in opposite directions rather than in the same direction (i.e. negative values of Ω_i/Ω_o). In the absence of diffusion, Poincaré plots indicate that better mixing is achieved with co-rotating cylinders than with counter-rotation (Chaiken *et al.* 1987). A similar result was seen here. For example, an effective Damköhler number of 19.05 occurs for $Pe_q = 5000$, $\Upsilon = 0.001$, $\epsilon = 0.5$, and $\Omega_i/\Omega_o = 6$ (co-rotation) versus a value of 9.20 for the equivalent counter-rotation case.

The period Υ_{max} for which the maximum deposition rate occurs is shown in figure 9. This optimum period is given by $\Upsilon_{max} = CPe_q^{-1}$ (where C is a constant) – at least for large Pe_q, equivalent to small diffusivities. This trend is consistent with the observation in the absence of diffusion that the extent of mixing depends only on the angular distance travelled during each period. However, the maximum deposition rate κ_{max} attainable depends upon Pe_q, increasing with increasing Pe_q, as seen in figure 10. While the extent of chaotic mixing is the same in each of these instances, the rate at which the mixing occurs varies with Pe_q. In the purely deterministic case the rate would vary linearly with angular velocity, but here, with diffusion present, the rate of increase is lessened, with the deposition rate varying approximately as $Pe_q^{0.25}$.

6.2. *Effective axial velocity*

Figure 11 illustrates the dependence of the mean axial solute velocity upon Pe_q for $\epsilon = 0.5$. For small Pe_q the average solute velocity $\bar{U}^*$ exceeds the mean annular 'Poiseuille' velocity $\bar{V}$ of the solvent for both continuous rotation of a single cylinder and successive alternate rotation of both. This is a consequence of the fact that the reaction at the outer cylinder removes solute from the slowest-moving axial streamlines, so that the only solute molecules to survive the trip downstream – and hence reach the exit of the system, where they are monitored – are those that have preferentially sampled the (faster-moving) axial streamlines existing near the centre of the annular space. As Pe_q is increased, the mean solute velocity decreases significantly for situations in which only the inner cylinder is rotated. In this circumstance, the recirculating flow near the reactive outer cylinder transports solute from some of the faster-moving axial streamlines to the reaction site, thereby decreasing the solute concentration along the faster streamlines, and hence reducing the average solute

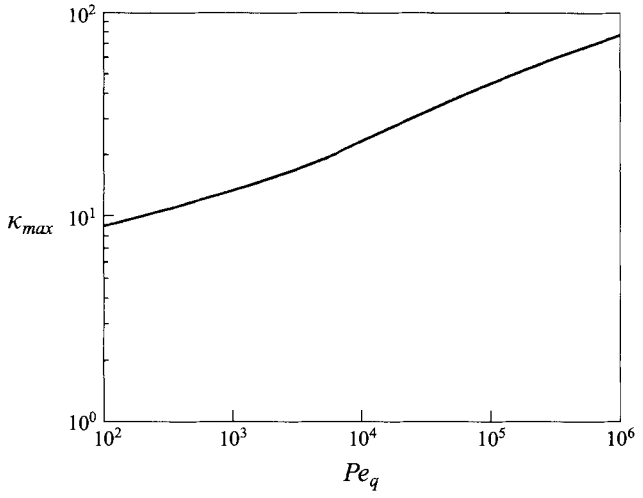

FIGURE 10. Dependence of the maximum achievable Damköhler number upon Pe_q, with $R_i/R_o = 0.3$, $\epsilon = 0.5$, $\Omega_i/\Omega_o = 6$.

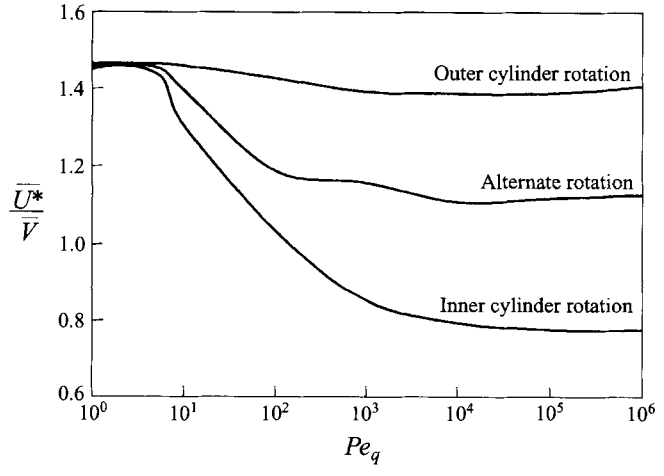

FIGURE 11. Dependence of the mean axial solute velocity upon Pe_q, with $R_i/R_o = 0.3$, $\epsilon = 0.5$, $\Omega_i/\Omega_o = 6$ and $\Upsilon = 0.01$.

velocity below that of the passive solvent carrier. In the case of rotation of the outer cylinder alone, $\bar{U}^*$exceeds $\bar{V}$ for all Pe_q because, as is true for small Pe_q, the solute is preferentially removed from the slower-moving streamlines. When the cylinders are rotated alternately with a period of $\Upsilon = 0.01$, the velocity ratio $\bar{U}^*/\bar{V}$ falls between the values for each of the cylinders rotating individually, ultimately attaining an asymptotic value of 1.1 for very large Pe_q. From these data it cannot be unequivocally established whether laminar chaos is the cause of the effective solute velocity approaching the perfectly mixed value of 1.0, or if rotating the cylinders alternately is simply causing this velocity to adopt a value intermediate between those attained by rotating each of the cylinders individually.

The transverse Péclet number dependence of the axial solute velocity at the optimum alternation period is illustrated in figure 12. For large Pe_q, the alternation period that maximizes the effective reaction rate is also the period at which the normalized

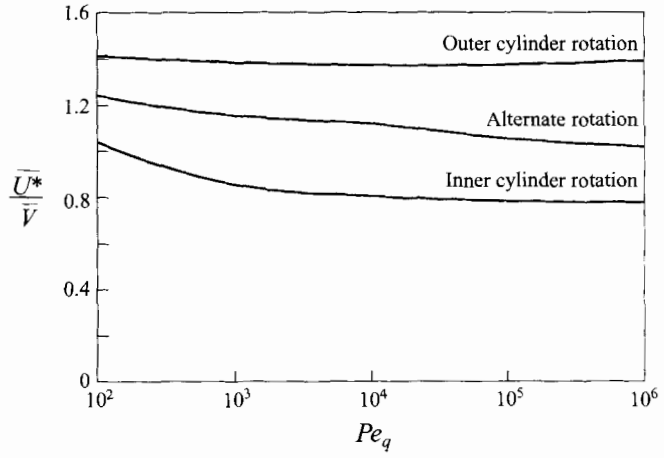

FIGURE 12. Effective solute velocity at the optimum rotation period, with $R_i/R_o = 0.3$, $\epsilon = 0.5$, and $\Omega_i/\Omega_o = 6$.

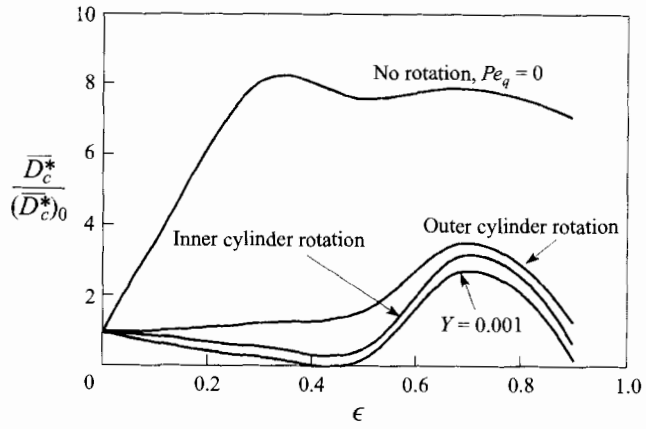

FIGURE 13. Dependence upon eccentricity of the ratio of the convective contribution $\bar{D}_c^*$ to the dispersivity to its value $(\bar{D}_c^*)_0$ for concentric cylinders in the absence of reaction and transverse flow, with $R_i/R_o = 0.3$, $Pe_q = 5000$ and $\Omega_i/\Omega_o = 6$.

solute velocity is closest to unity. For smaller Pe_q, the optimums differ only slightly from one another. In this figure, as in figure 11, the effective velocity when laminar chaos is present again lies between those for the individual single cylinder rotations, but here it is clearer that the effect of chaotic transport is to cause $\bar{U}^*/\bar{V}$ to approach the perfectly mixed value of 1.0.

6.3. *Convective dispersivity*

Figure 13 portrays the dimensionless convective contribution $\bar{D}_c^*/(\bar{D}_c^*)_0$ to the dispersivity, in which $(\bar{D}_c^*)_0$ represents the convective or Taylor dispersivity occurring for the case of concentric cylinders and in the absence of transverse flow. The diminution of solute concentration along the slower-moving streamlines resulting from reaction at the outer wall causes the dispersivity in the absence of transverse flow to be less than that observed by Sankarasubramanian & Gill (1971). In both that and the present work the dispersivity increases markedly as the eccentricity is increased. This phenomenon is caused by the increasing gradients arising in the axial velocity

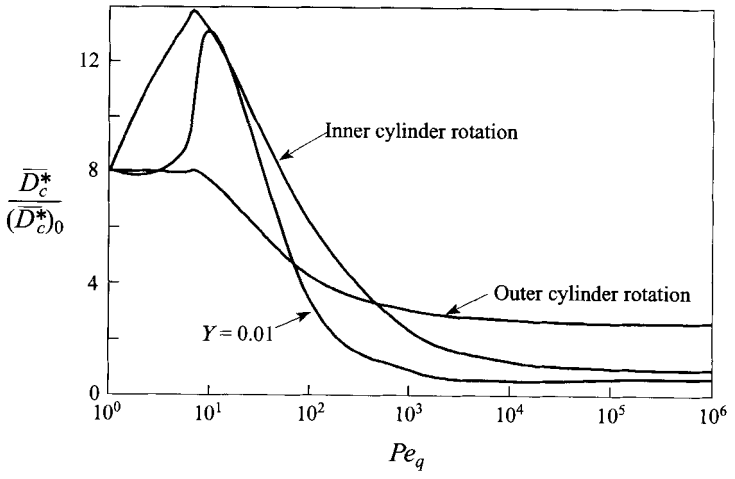

FIGURE 14. Dependence of the normalized convective Taylor contribution to the dispersivity upon Pe_q, with $R_i/R_o = 0.3$, $\epsilon = 0.5$, and $\Omega_i/\Omega_o = 6$.

profile with increasing eccentricity. The presence of steady transverse convection, as embodied in the pair of curves for the respective individual rotations of the inner and outer cylinders, acts to suppress most of this increase by allowing a solute particle to cross-sectionally sample the axial streamlines more rapidly. As evidenced by the $\Upsilon = 0.001$ data, the effect of laminar chaos is to further decrease the convective dispersion as a consequence of the enhanced transverse transport.

The Pe_q dependence of the convective dispersivity for $\epsilon = 0.5$ is shown in figure 14. At large Pe_q, when the cylinders are rotated alternately ($\Upsilon = 0.01$), the dispersivity achieves only about 5% of the value arising in the complete absence of rotation, and only one-half of the value attained when the inner cylinder is rotated continuously. For uniform rotation of the inner cylinder, as well as for alternate rotation of both cylinders, the Taylor dispersivity increases with Pe_q for small Péclet numbers, then subsequently decreases with further increases of Pe_q, as expected. This initial increase is caused by an enhancement in the probability of a tracer particle being found on one of the slower-moving streamlines, a result of the recirculation existing near the outer wall. For larger Pe_q this effect is ultimately overcome by the diminished time required for a solute particle to cross-sectionally sample all of the axial streamlines.

The convective dispersivity achieved at the optimum alternation period is displayed as a function of Pe_q in figure 15. The alternation period that maximizes the reaction rate is the same as that which minimizes dispersion for large Pe_q. While the dispersivities for continuous rotation of either of the cylinders reach asymptotic values for large transverse Péclet numbers, that for alternate rotation at the optimum period decays as approximately $Pe_q^{-0.65}$. Thus, the dispersivity under these circumstances is no longer inversely proportional to D, instead varying as $DPe_q^{-0.65}Pe_Q^2 \propto D^{-0.35}$. This behaviour is consistent with the results of Mezić, Brady & Wiggins (1996), which show that the axial dispersivity does not vary inversely with the molecular diffusivity when an ergotic transversal flow is present. However, the Pe_q dependence in this case is different than the $Pe \ln Pe$ dependence found by Jones & Young (1994) in the 'twisted-pipe' flow.

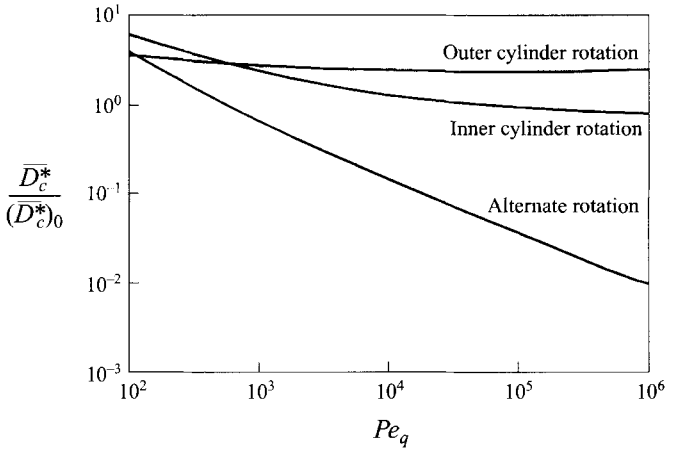

FIGURE 15. Dependence of the Taylor contribution to the dispersivity at the optimum alternation period upon Pe_q, with $R_i/R_o = 0.3$, $\epsilon = 0.5$, and $\Omega_i/\Omega_o = 6$.

7. Conclusions

In addition to affecting the three phenomenological macrotransport coefficients appearing in the macrotransport equation (4.4), the presence of chaotic advection also reduces the length of time required before the asymptotic description of the transport process embodied in (4.4) becomes applicable. In the absence of transverse convection, this description is valid only for times exceeding a characteristic cross-sectional diffusion time, $(R_o - R_i)^2/D$. For species with small diffusivities this restriction may be prohibitively long, allowing the solute particle to exit the duct (and hence be monitored) before the asymptotic theory described here becomes valid. By enhancing the lateral 'mixing' process, the presence of laminar chaos significantly reduces the amount of time required to reach this asymptotic state. For example, with the arbitrarily chosen spatially uniform initial condition used in our calculations, and for the case where rotation is absent and $\epsilon = 0.5$, the reaction-rate constant achieved a value lying within 1% of its ultimate asymptotic value in a dimensionless time interval of $\tau = 0.28$ following its introduction. This compares with the very much smaller times of 1.2×10^{-2} and 1.5×10^{-3} required to achieve the same 99% asymptote for alternation at the optimum frequency with $Pe_q = 10^4$ and 10^5, respectively. This finding is consistent with the analysis of Jones (1994), which showed that the time required for Taylor dispersion to be valid in the chaotic flow in a twisted pipe is $t \gg R/U \ln Pe$ rather than $t \gg R^2/D$ as for non-chaotic flow.

From the results presented here it is evident that laminar chaotic advection not only significantly enhances the *extent* of mixing of an inhomogeneous fluid, as has been previously demonstrated (Aref & Balachandar 1986; Chaiken *et al.* 1987; Swanson & Ottino 1990), but also increases the effective transverse transport *rate*. In particular, it is seen that the deposition or reaction rate may be enhanced at least several-fold over that achieved in the complete absence of transverse convection, or when one of the two cylinders is continuously and singly rotated. For $Pe_q = 5000$ the maximum reaction rate attainable is approximately 2.5 times that obtained for the purely diffusive case, or 30% greater than that attainable by rotating the inner cylinder singly (figure 5). For very large $Pe_q(10^6)$, the maximum deposition rate in the presence of laminar chaos (figure 10) is nearly five times that achieved solely by steady rotation of the

inner cylinder alone (figure 7), the maximum rate achievable by regular, non-chaotic, secondary convective transport.

Lateral transport enhancement is also observed to affect both the mean axial solute velocity and convective dispersivity. Explicitly, the effect of chaotic transport is to cause the mean value of the axial solute velocity through the annulus to approach that of the solvent, despite the selective removal of solute from the slower-moving axial streamlines. At the same time, the existence of laminar chaos acts to dramatically decrease the Taylor dispersivity by as much as several orders of magnitude over that achievable by non-chaotic advection. It was also noted that any change of parameters that serves to increase the deposition rate will, in most cases, decrease the dispersivity, although this is not always the case. The most notable exception occurs at small Pe_q, where the dispersivity increases with increasing Pe_q, simultaneously with the deposition rate. These differences in behaviour arise from the fact that whereas the deposition rate depends exclusively on cross-sectional transport, the axial dispersivity depends jointly on both the transverse and axial transport. Therefore, for one seeking a computational means of evaluating the mixing effectiveness of a given flow field, the deposition rate is the most sensitive of the three possible phenomenological measures by virtue of its exclusive dependence on the transverse transport processes.

Poincaré maps, while providing a qualitative view of the extent of chaotic transport, as well as a visual image of which regions of the flow are affected by laminar chaos, furnish no directly usable engineering design information regarding the transverse transport rate (Swanson & Ottino 1990). In contrast, the present work provides a quantitative measure of the degree of transport enhancement arising from the presence of chaotic advection. In particular, Poincaré sections indicate that, in general, longer switching periods lead to a greater extent of mixing. Here, it was found that an optimum alternation frequency exists with respect to the transport rate. Moreover, our analysis incorporates the effect of molecular diffusion, demonstrating that even at very large transverse Péclet numbers, the presence of molecular diffusion can significantly affect the transport rate beyond that occasioned by convection (i.e. laminar chaos) alone, provided that sufficient time is allowed. On a broader theme, quantitative understanding of the interaction between molecular diffusion and laminar chaos may have important ramifications in elaborating the much debated (Glotefety, Taylor & Zoller 1983) role of molecular diffusion in turbulent chaos.

This work was supported by a National Science Foundation Graduate Fellowship to M.D.B. and by a grant to H.B. from the Office of Basic Energy Sciences of the US Department of Energy.

REFERENCES

AREF, H. & BALACHANDAR, S. 1986 Chaotic advection in a Stokes flow. *Phys. Fluids* **29**, 3515–3521.

BALLAL, B. Y. & RIVLIN, R. S. 1976 Flow of a Newtonian fluid between eccentric rotating cylinders: inertial effects. *Arch. Rat. Mech. Anal.* **62**, 237–294.

CHAIKEN, J., CHU, C. K., TABOR, M. & TAN, Q. M. 1987 Lagrangian turbulence and spatial complexity in a Stokes flow. *Phys. Fluids* **30**, 687–694.

GHOSH, S., CHANG, H. -C. & SEN, M. 1992 Heat-transfer enhancement due to slender recirculation and chaotic transport between counter-rotating eccentric cylinders. *J. Fluid Mech.* **238**, 119–154.

GLOTEFETY, D. E., TAYLOR, A. E. & ZOLLER, W. H. 1983 Atmospheric dispersion of vapors: Are molecular properties unimportant? *Science* **219**, 843–845.

HAPPEL, J. & BRENNER, H. 1983 *Low Reynolds Number Hydrodynamics*. Kluwer.

JANA, S. C. & OTTINO, J. M. 1992 Chaos-enhanced transport in cellular flows. *Phil. Trans. R. Soc. Lond.* A **338**, 519–532.

JANSSEN, L. A. M. 1976 Axial dispersion in laminar flow through coiled tubes. *Chem. Engng Sci.* **31**, 215–218.

JOHNSON, M. & KAMM, R. D. 1986 Numerical studies of steady flow dispersion at low Dean number in a gently curving tube. *J. Fluid Mech.* **172**, 329–345.

JONES, S. W. 1994 Interaction of chaotic advection and diffusion. *Chaos, Solitons, & Fractals* **4**, 929–940

JONES, S. W. & YOUNG, W. R. 1994 Shear dispersion and anomalous diffusion by chaotic advection. *J. Fluid Mech.* **280**, 149–172.

KAPER, T. J. & WIGGINS, S. 1993 An analytical study of transport in Stokes flows exhibiting large-scale chaos in the eccentric journal bearing. *J. Fluid Mech.* **253**, 211–243.

KUSCH, H. A. & OTTINO, J. M. 1992 Experiments on mixing in continuous chaotic flows. *J. Fluid Mech.* **236** 319–348.

MEZIĆ, I., BRADY, J. F. & WIGGINS, S. 1996 Maximal effective diffusivity for time periodic incompressible fluid flows. *SIAM J. Appl. Maths* **56**, 40–56.

NUNGE, R. J., LIN, T. -S. & GILL, W. N. 1972 Laminar dispersion in curved tubes and channels. *J. Fluid Mech.* **51**, 363–383.

OTTINO, J. M. 1990 Mixing, chaotic advection, and turbulence. *Ann. Rev. Fluid Mech.* **22**, 207–253.

OTTINO, J. M., MUZZIO, F. J., TJAHJADI, M., FRANJIONE, J. G., JANA, S. C. & KUSCH, H. A. 1992 Chaos, symmetry, and self-similarity: Exploiting order and disorder in mixing processes. *Science* **257**, 754–760.

PIERCY, N. A. V., HOOPER, M. S. & WINNEY, H. F. 1933 Viscous flow through pipes with cores. *Phil. Mag.* **15**, 647–676.

SAN ANDRES, A. & SZERI, A. Z. 1984 Flow between eccentric rotating cylinders. *Trans. ASME* E: *J. Appl. Mech.* **51**, 869–879.

SANKARASUBRAMANIAN, R. & GILL, W. N. 1971 Taylor dispersion in laminar flow in an eccentric annulus. *Intl. J. Heat Mass Transfer* **14**, 905–919.

SHAPIRO, M. & BRENNER, H. 1986 A reactive Taylor dispersion model of aerosol collection by fibrous and granular filters. *Proc. 1986 CRDEC Conference on Obscuration and Aerosol Reseach.* Chemical Research, Development and Engineering Center, US Army, Edgewood, Maryland.

SHAPIRO, M. & BRENNER, H. 1990 Taylor dispersion in the presence of time-periodic convection phenomena. Part 1. Local-space periodicity. *Phys. Fluids* A **10**, 1731–1743.

SHAPIRO, M., KETTNER, I. J. & BRENNER, H. 1991 Transport mechanics and collection of submicrometer particles in fibrous filters. *J. Aerosol Sci.* **22**, 707–722.

SNYDER, W. T. & GOLDSTEIN, G. A. 1965 An analysis of fully developed laminar flow in an eccentric annulus. *AIChE J.* **11**, 462–467.

SWANSON, P. D. & OTTINO, J. M. 1990 A comparative computational and experimental study of chaotic mixing of viscous fluids. *J. Fluid Mech.* **213**, 227–249.

TAYLOR, G. I. 1953 Dispersion of soluble matter in solvent flowing slowly through a tube. *Proc. R. Soc. Lond.* A **219**, 186–203.